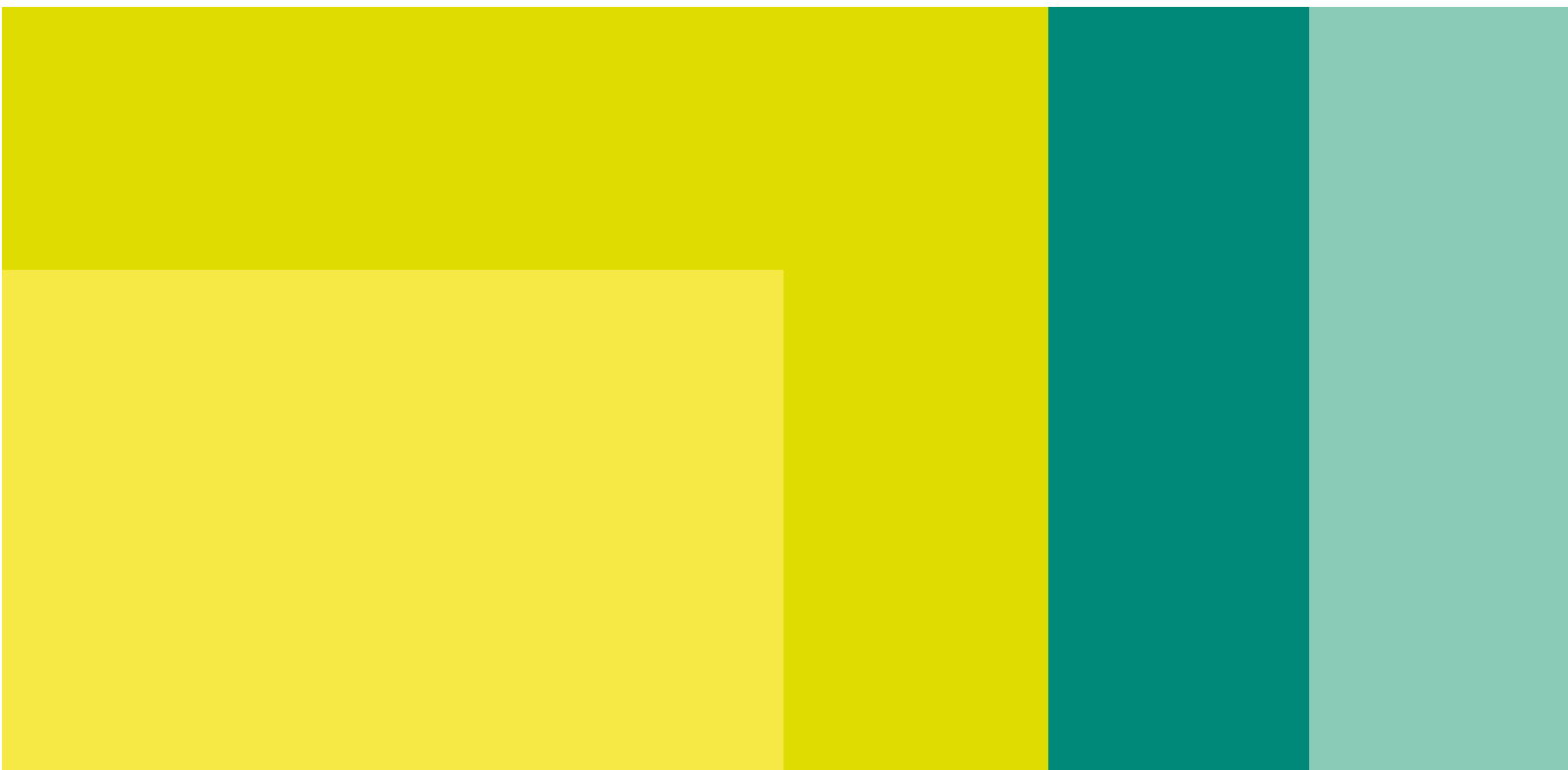Sven Kock, Mariela Tapia, Christopher Varela, Matthias Schirmer

Spatio-temporal evaluation of green hydrogen production in Ecuador

artec
Forschungszentrum
Nachhaltigkeit

Das artec Forschungszentrum Nachhaltigkeit ist ein interdisziplinäres Zentrum der Universität Bremen zur wissenschaftlichen Erforschung von Fragen der Nachhaltigkeit. In seiner Schriftenreihe „artec-Paper" gibt das Forschungszentrum in loser Folge Aufsätze und Vorträge von Mitarbeiter:innen sowie ausgewählte Arbeitspapiere und Berichte von Forschungsprojekten heraus.

Impressum

Spatio-temporal evaluation of green hydrogen production in Ecuador

Sven Kock [a], Mariela Tapia [b] [*], Christopher Varela [c], Matthias Schirmer [a]

[a] Department of Industrial Engineering, Ernst-Abbe-Hochschule Jena, Jena, Germany
[b] Resilient Energy Systems Research Group, University of Bremen, Bremen, Germany
[c] FCNM-CERA, Escuela Politécnica del Litoral, Guayaquil, Ecuador
[a] Department of Industrial Engineering, Ernst-Abbe-Hochschule Jena, Jena, Germany

* Corresponding author: mariela.tapia@uni-bremen.de

Abstract

This study evaluates the techno-economic conditions of green hydrogen production based on the combined operation of geographically-dispersed and complementary wind and solar power farms in Ecuador. Representative sites with high potential of wind and solar resources are used for the calculations. The hourly meteorological data of these sites is used to simulate the power output of solar photovoltaic (PV) and wind power farms. Then, based on the renewable power output and the associated generation cost, the production of hydrogen is simulated using an electrolysis optimization model. Using a set of indicators, we evaluate the results of three combinations of different PV and wind farms to identify the relation between the renewable power and the hydrogen production and cost. Results show that all combinations produce green hydrogen at a levelized cost of hydrogen (LCOH) of less than US$4 per kg. It is found that the LCOH can be related to the hourly variation and the cost of the renewable generation. This means that the higher the stability of the renewable power output, the lower the simulated LCOH. We will use the findings of this study to evaluate the performance with more combinations of PV and wind power farms in a future work.

Introduction

The transition to sustainable energy systems requires high shares of renewable power and flexible storage alternatives. Hydrogen produced through the water electrolysis, called green hydrogen, can store renewable energy and supply it to energy-intensive sectors. Green hydrogen can replace gray hydrogen, which is primarily used for ammonia production in nitrogen fertilizers (Alavijeh et al., 2020), thereby reducing the greenhouse gas emissions of the process (Smith et al., 2020). It can also be used as a reducing agent in steel production, replacing fossil reactants thus reducing carbon emissions (Müller-Markus et al., 2023; Oliveira et al., 2021). Additionally, it can be used as an energy storage and transportation vector, with the potential to power various sectors, including aviation, shipping, and heavy freight road logistics (Abdin et al., 2020).

In view of these opportunities, green hydrogen is seen as a key feature for sustainable development planning in several countries. In the case of Ecuador, the government released in 2023 a roadmap for the production and use of green hydrogen as 'one decisive starting point to promote a just energy transition' (Ministerio de Energía y Minas, 2023, p. 9). This strategy aims to install 6 GW of electrolysis capacity by 2050 to produce hydrogen for domestic consumption and export.

Ecuador has vast potential of hydrological resources in the Amazon and Pacific basins, and the deployment of the untapped potential is at the core of the national energy strategy (IHA, 2017; MERNNR, 2018). The Ecuadorian power mix is highly dominated by hydropower (62.4 % of the total share in 2023 (ARCERNNR, 2024)), which could represent great opportunities for the production of green hydrogen (IHA, 2021). However, since the end of 2023 Ecuador is the midst of a severe energy crisis due to a historic drought in the Amazon basin, aggravated by inadequate expansion of generation capacity and lack of power plant maintenance. As a result, the country has experienced power shortages of several hours per day, causing serious socio-economic impacts (González, 2024). Therefore, the vulnerability of hydropower to extreme weather conditions could jeopardize a possible production of green hydrogen as well.

Ecuador also has great potential of solar and wind resources (CONELEC, 2008; MEER, 2013). However, the deployment of these technologies in the country is still at an early stage, with a share of only 1.2% of the power mix in 2023 (ARCERNNR, 2024). According to Tapia (2023), solar and wind power have a great potential to complement hydropower during the dry periods. The author also identified important spatio-temporal synergies between solar and wind power. It was found that the joint operation of geographically-dispersed solar photovoltaic (PV) and wind power systems reduces the intrinsic variability of each resource. Furthermore, the study found that wind power from high resource

sites stabilizes PV power output at diurnal timescales during the windy months (June–September), suggesting that both technologies could serve as baseload during this period, thus reducing the requirements for energy storage (Tapia, 2023).

Based on the findings of Tapia (2023), in this study, we evaluate the techno-economic conditions of hydrogen production from geographically-dispersed and complementary solar PV and wind power in Ecuador. We use hourly meteorological data of representative sites with high resource potential to simulated the power output. Using an electrolysis optimization model, the hydrogen production is simulated based on the solar and wind power feed-in time series. Then, we select a sample of combinations of PV and wind power farms and evaluate their performance based on a set of indicators. In the following section, the data and methods used for the evaluation are described. Then, the results are presented and discussed. Finally, we draw some conclusions and give an outlook for future work.

Data and methods

Meteorological data

For this study, we used the results of the spatio-temporal characterization of solar and wind resources in Ecuador developed by Tapia (2023). Her work identified 22 subregions that characterize the solar resources and 10 subregions that characterize the wind resources. The meteorological data of one representative site from each of the solar subregions, as well as from the six wind subregions along the Andes, where the highest wind potential lies, was made available. These sites represent the best locations in their respective subregion.

The solar data comprises the long-term hourly averages at 3 × 3 km grid resolution of global horizontal irradiance (GHI), diffuse horizontal irradiance (DHI), direct normal irradiance (DNI) in [W/m2], wind speed in [m/s] and ambient temperature in [℃] over Ecuador's mainland. The long-term averages were calculated based on data from 1998 to 2018, which was retrieved from the National Solar Radiation Database (Sengupta et al., 2018). See more details in Tapia, Heinemann, et al., (2022).

The wind data comprises the long-term hourly averages at 3 × 3 km grid resolution of wind speed [m/s] and the temperature [K] both at a height of 80 m above ground level (AGL), surface air density [kg/m³], surface air pressure [Pa] and surface roughness length [m]. The long-term averages were calculated based on data from 2005 to 2018, which was simulated using the Weather and Forecast Research mesoscale model. See more details in Tapia (2023).

Fig. 1 shows the geographic location of the representative sites, which are the grid points with the highest solar radiation and wind speed within each subregion. These sites were selected by Tapia (2023) through a Geographic Information System (GIS) based approach to determine the geographic area suitable for the deployment of utility-scale solar PV and wind power farms after applying a set of excluding criteria. See more details in Tapia (2023).
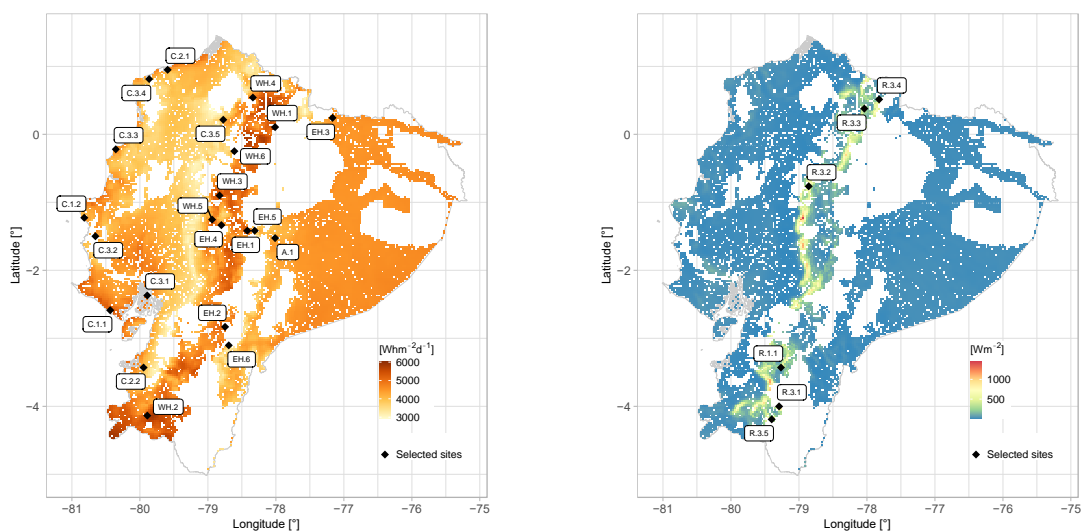
Fig. 1. Long-term annual mean daily total GHI (left) and long-term annual mean wind power density at 80 mAGL (right) of suitable area after applying the GIS-based approach using constraint layers concerning infrastructure, water bodies, and protected areas (See more details in Tapia (2023)). The grid cells that have the highest value within each solar or wind subregion are marked in black and labeled according to the subregion's name. The solar subregions are labeled as A.1 in the Amazon, C.X.X on the coast, EH.X in the eastern Andes, and WH.X in the western Andes. The wind subregions are labeled as R.1.X and R.3.X. Source (Tapia, 2023, Chapter 5).

Solar PV system simulation

Following the methodology performed by Tapia, Ramos, et al.(2022), the *pvlib-python* package (Anderson et al., 2023) is used to simulate the power output of a solar PV farm at each solar site. The PV farm consist of mono-crystalline silicon modules *JAM78-S30-580-MR* from JA Solar and the inverter *Sunny Central 4600 UP* from SMA. Both are state-of-the-art components suitable for utility-scale PV systems.

For the simulations, the surface azimuth is set at 90° respect to due north and the tilt angle is set at 10°, which is the optimal module orientation according to a previous sensitivity analysis of the rooftop PV technical potential in three cities of Ecuador's mainland, reported in Tapia, Ramos, et al. (2022). The system losses are set to 14%, which include losses due to soiling, shading, mismatching, wiring, connections, light induced degradation, nameplate rating and operational availability (Dobos, 2014). Losses due to temperature are modeled using the PVsyst model (Sauer et al., 2015) The Hay-Davies model (Hay & Davies, 1980) is selected as the irradiance transposition model. The PVsyst DC-model (Mermoud, 2014) is used to calculate the power output of the PV modules. The technical parameters of the PV modules and inverter are retrieved from the component datasheets (JaSolar, n.d.; SMA, n.d.) and the PVSyst software database (Mermoud, 2014). The AC output of the inverter is calculated using the PVWatts-Model (Dobos, 2014).

To determine the capacity of the PV farm at each site, we consider that approximately 100 MW of PV capacity can be installed per km² (Umweltbundesamt, 2023; Wesselak & Schabbach, 2009, Chapter 4.4.3). We also assume that 10% of the total surface in each grid cell of 9 km² is available for construction of the PV farm. Under these assumptions, for this study the installed capacity of the PV farm at each solar site is 90 MW.

Wind power system simulation

Following the methodology performed by Tapia (2023), the python package *windpowerlib* (Haas et al., 2024) is used to simulate the output of a wind farm at each wind site. We use the same wind turbine types as in Tapia (2023, Chapter 5), which were selected depending on the long-term annual mean wind speed at 80 m AGL of each selected site, as shown in Table 1.

Table 1: Long-term annual mean wind speed and wind power density at selected sites in each wind subregion and specifications of the wind turbines used to simulate the power output of a wind farm at each site. Source: (Tapia, 2023, Chapter 5).

Subregion	Mean wind speed at 80 mAGL [m/s]	Mean wind power density at 80 mAGL [W/m²]	Turbine model (Wind class)	Manufacturer
R.3.1	10.95	1420.06	V112-3.45 (IEC IA)	Vestas
R.3.2	8.63	821.57	V117-3.45 (IEC IIA – IB)	Vestas
R.3.3	5.91	258.34	GE 3.2-130 (IEC IIIA)	General Electric
R.3.4	5.23	186.37	GE 3.2-130 (IEC IIIA)	General Electric
R.3.5	6.54	336.58	GE 3.2-130 (IEC IIIA)	General Electric
R.1.1	4.60	148.72	GE 3.2-130 (IEC IIIA)	General Electric

The capacity of each wind farm is determined according to the number of turbines that could be installed in a given area. For this, it is assumed that the wind turbines are positioned with a distance of $10R \cdot 3R$, where R is the impeller diameter in [m] (Wang et al., 2022). Thus, the number of turbines $n_{Turbines}$ is calculated according to Eq. 1, where LUF_{wind} [%] is the land use factor that is used to define how much of the surface A in a grid cell of 9 km² could be used for the construction of a wind farm. The impeller diameter R is calculated using a correlation between the hub height h_{Hub} [m] and the impeller diameter as in Van Sark et al. (2019), according to Eq. 2. We consider $LUF_{wind} = 20\%$ for each wind farm, which results in an installed capacity of 28.8 or 29.7 MW per wind site.

$$n_{\text{Turbines}} = \frac{LUF_{\text{wind}} * A}{10 * 3 * R^2} \tag{1}$$

$$R = \frac{h_{\text{Hub}} - 15}{0.79} \tag{2}$$

Combination of geographic dispersed power systems

The aim of this study is to evaluate the generation of hydrogen from the combined operation of PV and wind power farms in different geographic locations. The total number of possible combinations of k elements from a set of n elements ($k, n \in N$) without repetitions and where the order is irrelevant can be calculated using the binomial coefficient (Behrends, 2013). Applied to this study, this represents the number of possible combinations with k out of $n = 28$ wind and solar sites. By calculating the sum of the binomial coefficients for $k \in [1,28]$, it can be determined that the total number of possible combinations is 2.7E+08.

Since performing this number of simulations would require high computational power, in this study we select a sample of combinations and evaluate their performance using a set of indicators. The selection of the combination sample is based on the results of the correlation analysis of solar and wind resources reported in Tapia (2023, Chapter 4). We select three combinations with those sites that have a pairwise negative Pearson correlation coefficient $\rho \leq -0.7$, which is interpreted as strong complementary behavior. The combinations are listed and described in Table 2.

Table 2: List of sites and description of Combinations A (see location in Fig. 1)

Combination	Description	Sites
A1	Solar sites on the coast and in the western Andean highlands	C.1.2, WH.3, WH5
A2	Solar sites in the eastern Andean highlands and wind sites from region R3	EH.2, EH.4, R.3.1, R.3.2
A3	Solar sites on the coast and wind sites from region R1 and R3	C.1.1, C.1.2, R.1.1, R.3.5

Set of indicators

We use a set of indicators to evaluate the performance of the combinations in terms of the relation between the feed-in time series of the PV and wind power farms and the hydrogen production and costs. They are an intent to relate the effectiveness of green hydrogen production to the characteristics of the renewable energy generation of the selected combinations. Also, they may help to estimate how well some of the other combinations work without having to simulate all of them. We use the following four indicators:

1) *Hourly coefficient of variation (CV_h)*: It is used to assess the dispersion of the feed-in time series of the PV and wind power farms. Lower dispersion translates to more stable power output, which is beneficial for the performance of electrolyzers (Bockelmann et al., 2024). This coefficient is relative to the total volume, ensuring that the result is not distorted by the production capacity (Hartung et al., 2005). This is important because if more total energy is produced, the total dispersion is higher as well. The CV_h, $[-]$ is calculated according to Eq. 3, where σ_{hour} is the standard derivation of the hourly power generation and $\overline{E_{el}}$ is the mean electricity production.

$$CV_h = \frac{\sigma_{hour}}{\overline{E_{el}}} \tag{3}$$

2) *Daily coefficient of variation (CV_{24})*: the variation of the daily average power output CV_{24}, $[-]$ is calculated according to Eq. 4. This metric is included because high daily variations are expected due to the solar plants. This means that seasonal variations are not captured by CV_h, although they may cause that considerable electrolysis capacity is not usable over a long timescale. By using both coefficients CV_h and the CV_{24}, we can see if seasonal variations of renewable generation impact the hydrogen production.

$$CV_{24} = \frac{\sigma_{day}}{\overline{E_{el}}} \tag{4}$$

3) *Levelized Cost of Electricity (LCOE)*: The cost of electricity, measured as LCOE, is considered in the optimization model and has a direct impact on the hydrogen cost. The lower the cost of electricity for electrolysis, the lower the cost of hydrogen production. LCOE is calculate according to Eq. 5, which is an adaptation of the formula of the annuity method explained among others by Kost et al. (2021, Chapter 8). It includes a degradation factor and multiplies reference values from the literature listed in Table 3 to the total installed capacity.

$$LCOE = \frac{P_{Max} * (CapEx_{rel} * ANF + OpEx_{rel})}{E_{el} * (1 - DF)} \tag{5}$$

where,

P_{Max} [kW]: Total installed capacity

$CapEx_{rel}$ [US$/kW]: Capital expenditures relative to the installed capacity

$OpEx_{rel}$ [US$/kW/a]: Annual operation and maintenance expenditures relative to the installed capacity

E_{el} [kWh]: Annual energy generation

DF [%]: Degradation factor

ANF [1/a]: Annuity factor calculated according to Eq. 6.

$$ANF = \frac{WACC * (1 + WACC)^n}{(1 + WACC)^n - 1}$$

(6)

where,

WACC [%]: Weighted average cost of capital

n [a]: Power plant lifetime

Table 3: Economical parameters for the base setup.

Parameter	Value	Source
CapEx$_{rel, solar}$	860 [US$/kW] [a]	(IRENA, 2023)
CapEx$_{rel, wind}$	1305 [US$/kW] [b]	(IRENA, 2023)
OpEx$_{rel, solar}$	7.4 [US$/kW/a] [b]	(IRENA, 2023)
OpEx$_{rel, wind}$	20 [US$/kW/a] [c]	(IRENA, 2023)
WACC	10 [%]	(Steffen, 2020)
Lifetime, solar	25 [a]	(JaSolar, n.d.)
Lifetime, wind	20 [a]	(Decker et al., 2019)
DF, solar	0.61 [%]	(JaSolar, n.d.)
DF, wind	1.6 [%]	(Staffell & Green, 2014)

Notes: [a] average value of utility-scale solar PV systems installed costs in 2022 for Argentina, Chile and Brazil. [b] Weighted average value in 2022 for South America. [c] Value for Brazil in 2022.

4) *Full load hours (FLH)*: The FLH is the quotient of the annual energy yield and the installed capacity. It indicates how much time the power plant would have to operate on full load in order to yield its annual energy output. It is a common indicator of the effectiveness of renewable energy systems. The higher the FLH, the higher the energy production per installed capacity (Mertens, 2020, Chapter 2.2.3; Wesselak & Schabbach, 2009, Chapter 2.3).

Electrolysis simulation

We use the optimization model developed by Varela et al. (2023) to simulate of the hydrogen production. The model inputs power supply time series and associated LCOE to optimize the operation schedule of a given number of alkaline electrolyzers (AEL) and to identify the lowest possible cost, named Levelized Cost of Hydrogen (LCOH, [US$/kg]). For the simulation, the model mathematically describes the characteristics and the different operational states of the AEL. Descriptions of the transition between the different operational states are also included, meaning that the sensitivity of AEL to power input variation is considered. This aspect is relevant for the production of green hydrogen from variable renewable power.

The model requires the following modifications for the application in this study. First, the input parameters of the AEL need to be defined. The power input $P_{total}(t)$, [MW] is calculated according to Eq. 7, where $P_i(t)$, [MW] is the output of the PV and/or wind power farm of site i included in a given combination.

$$P_{total}(t) = \sum_i P_i(t)$$

(7)

The associated $LCOE$ of the input power $LCOE_{WA}$, [$/kWh] is defined as the weighted average of the calculated LCOEs of all sites in a given combination and calculated according to Eq. 8, where $LCOE_i$ is the levelized cost of electricity of the site i; E_i, [MWh] is their annual energy generation of site i; and E_{total}, [MWh] is the total annual energy generation of all sites in a given combination.

$$LCOE_{WA} = \sum_i LCOE_i * \frac{E_i}{E_{total}}$$

(8)

In contrast to Varela et al. (2023), this study does not consider electricity from the grid. Therefore, the grid load was defined as zero and no grid emission factors were included in the model. Consequently, the emission costs in the calculation of the $LCOH$ were also left unconsidered. Because of this, the $LCOH$ is uniquely determined by the investment costs for the electrolyzers (C_{inv}, $[US\$]$) divided by their lifetime (n_{elec}, $[a]$), as well as the cost of all the electricity used, (C_{el}, $[US\$/a]$), the total annual costs of the startups (C_{st}, $[US\$/a]$), and the annual hydrogen production (m_{H2}, $[kg/a]$), according to Eq. 9.

$$LCOH = \frac{\frac{C_{inv}}{n_{elec}} + C_{el} + C_{st}}{m_{H2}} \qquad (9)$$

Since the investment and the startup costs are given in Euros and the other parameters in this study are given in US\$, they are converted by applying the average conversion factor of the last 10 years provided by European Central Bank (2024). This means that one Euro has the same value as 1.1267 US\$. After the conversion, the relative investment cost for the electrolyzers is 711 US\$/kW. The optimization model remains unchanged except for the aforementioned modifications.

For the simulations, we assume that the electrolysis capacity is 20% of the installed renewable energy capacity. Thus, the number of electrolyzers is calculated according to Eq. 10, where P_{RE} $[MW]$ is the installed renewable energy capacity of a given combination and P_{Elec} $[MW]$ is the maximum power of one electrolyzer.

$$n_{Elec} = \frac{P_{RE} * 20\%}{P_{Elec}} \qquad (10)$$

Results and discussion

Table 4 shows the results of the indicators for the combinations A1, A2, and A3. It can be seen that combination A1, which comprises only solar sites, shows the highest installed capacity. Combination A2 shows the highest FLH, as this combination includes the site with the best wind resources (R.3.1). Combinations A1 and A2 produce a similar amount of energy at a lower LCOE compared to that of combination A3. Regarding the coefficient of variation, it is observed that combination A2 has a lower CV_h compared to that of combinations A1 and A3. Meanwhile, combination A1 presents the best coefficient of variation when the daily fluctuations are not considered (CV_{24}).

Table 4: Result of the indicators for combinations A

Indicator	Combination A1 (Sites: C.1.2, WH.3, WH5)	Combination A2 (Sites: EH.2, EH.4, R.3.1, R.3.2)	Combination A3 Sites: (C.1.1, C.1.2, R.1.1, R.3.5)
Installed capacity [MW]	270	238.5	237.6
E_{el} produced [GWh]	762.3	718.8	613.3
FLH [h]	2823	3014	2581
LCOE [\$/MWh]	36.40	39.61	46.18
CV_h [-]	1.28	0.97	1.16
CV_{24} [-]	0.07	0.17	0.12

Table 5 shows the simulation results of the hydrogen production using the renewable resources of the different combinations. It can be seen that combination A2 produces more hydrogen at a lower LCOH compared to the other combinations. Even though combination A2 has a higher CV_{24} and LCOE than combination A1, its LCOH is lower. Thus, the only parameter that indicates that A2 may perform better is the CV_h. It is observed that the lower the CV_h in Table 4 is, the higher the relative energy use of the combinations in Table 5.

Table 5: Electrolysis simulation results for combinations A

Parameter	Combination A1 (Sites: C.1.2, WH.3, WH5)	Combination A2 (Sites: EH.2, EH.4, R.3.1, R.3.2)	Combination A3 Sites: (C.1.1, C.1.2, R.1.1, R.3.5)
Number of Electrolyzers	18	16	16
E_{el} used [GWh]	215.5	297.3	231.7
E_{el} used [%]	28.3	41.4	37.8
FLH_{elec} [h]	3856	5985	4664
H_2 Produced [t]	4124	5681	4426
LCOH [US\$/kg]	3.28	2.93	3.54

To understand this indicator in more detailed, Fig. 2 displays the power output of the three combinations during the first week of the year. On the one hand, combination A1, which has the highest CV_h, presents a high daily fluctuation. This is because this combination only includes solar power plants that do not generate at nighttime. For the electrolysis, this means that for around half of the time, none of the installed capacity can be used. Therefore, the relative output is reduced and the cost increases. On the other hand, combinations A2 and A3, which include solar and wind power plants, deliver at least a share of the daily electricity supply at nighttime, meaning that they present a lower CV_h and a higher relative energy use.
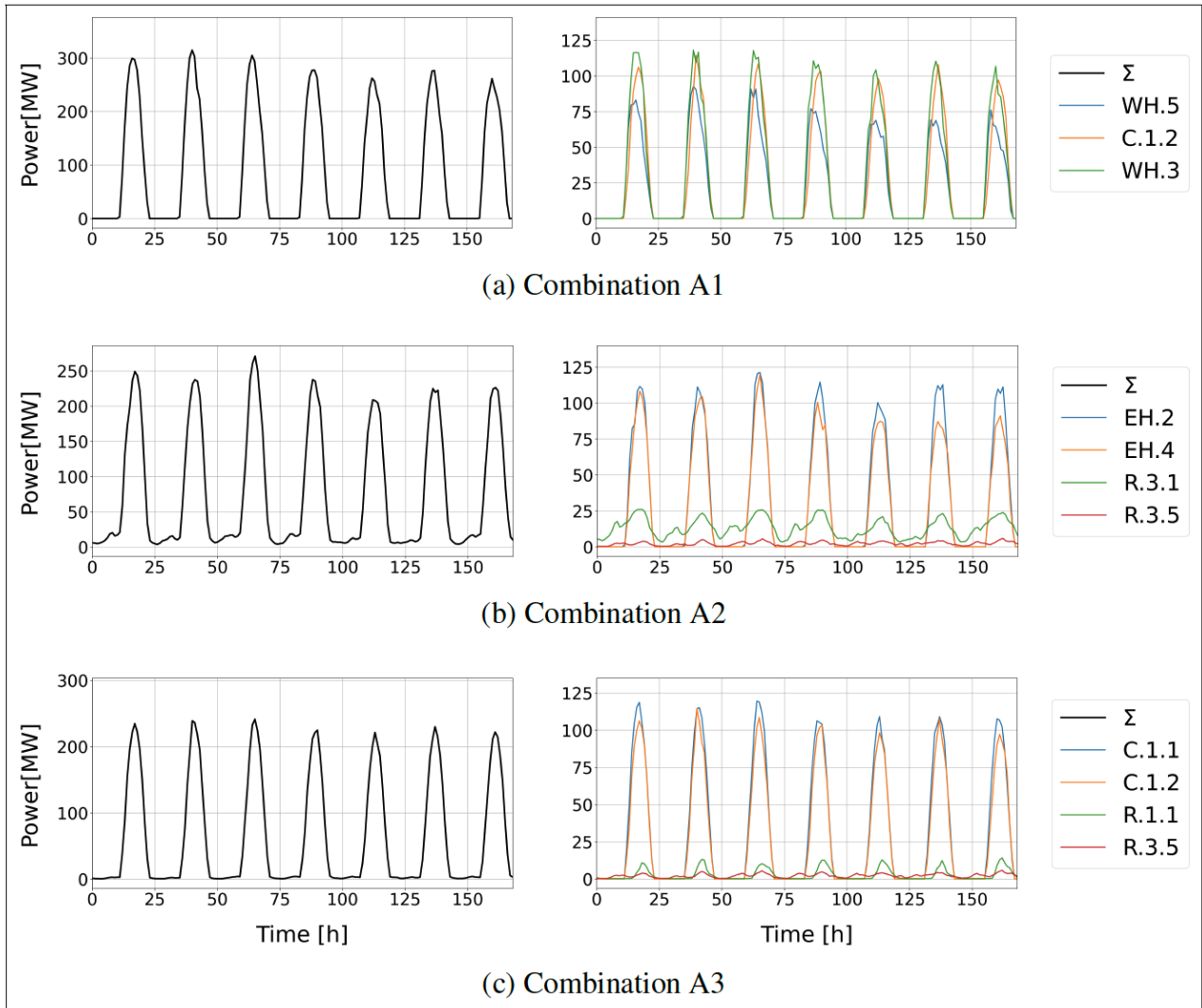

Fig. 2: Power output of combinations A during the first week of the year. Time is in UTC. On the left: Combined power output. On the right: Power output per site.

The stability measured by the CV_h can also be observed in Fig. 3. Here, the yearly duration curves of the combinations are presented and the installed electrolysis capacity is shown. It can be seen that all combinations allow the installed electrolysis capacity to be used for less than 4000 hours. However, after crossing that point, combination A2 has a significantly flatter curve compared to that of A1 and A3. In fact, combination A1 provides no energy for more than half of the year, confirming the observation made in Fig. 2. On the other hand, combination A2, which has the lowest CV_h, can provide around ten percent of the energy for almost 6000 hours of the year. Therefore, although the relative electrolysis capacity of the two combinations is similar, the electrolyzers can operate 55% longer when supplied by combination A2 than when supplied by combination A1.
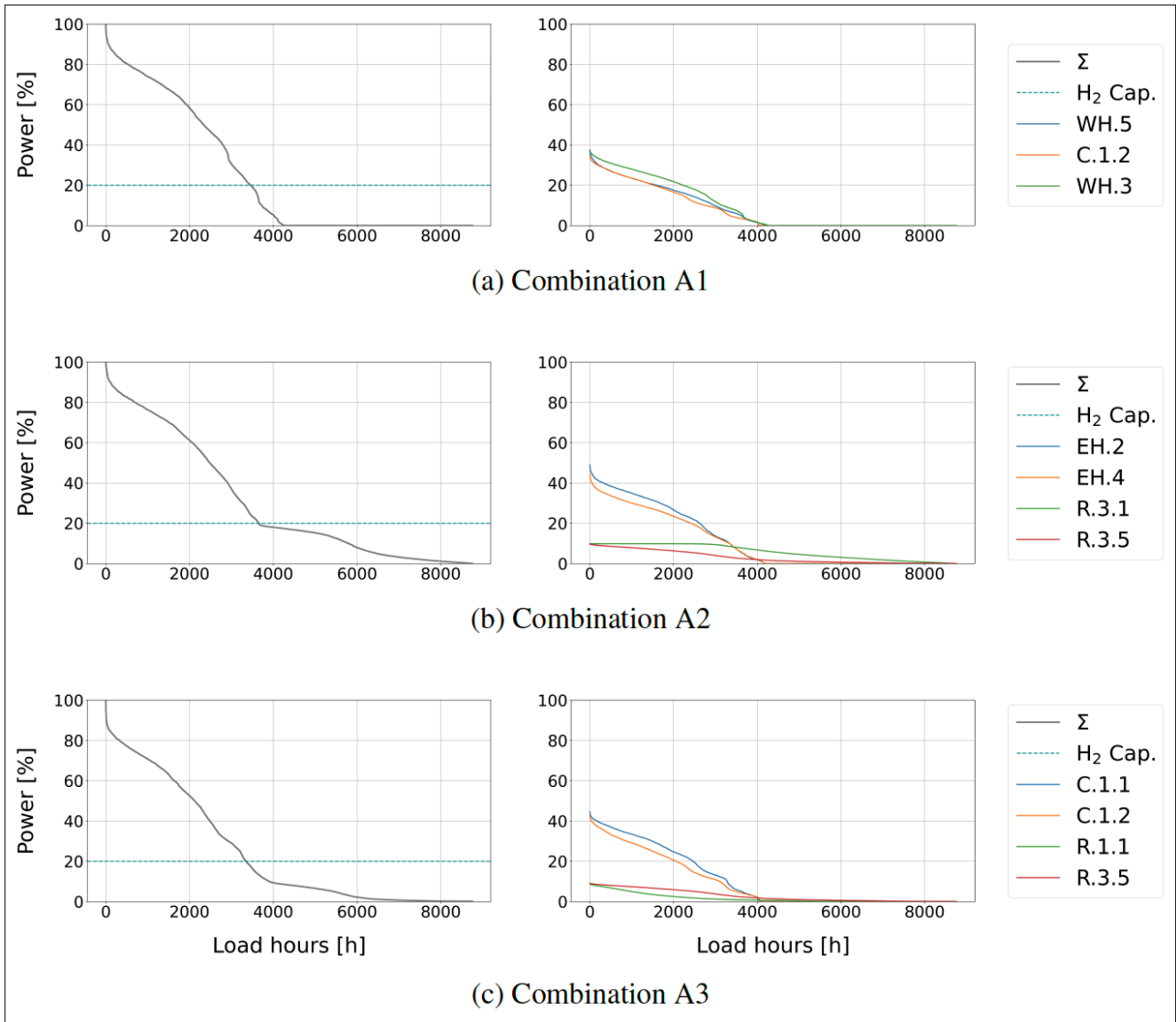
Fig. 3: Yearly duration curves of the combinations A. On the left: Duration curve of the combination, where the dotted line represents the electrolysis capacity (20%). On the right: Duration curves per site.

The meaning of the dispersion measured by the CV_{24} can be observed in Fig. 4, where the 24-hour average power generation of all the year is presented. It is observed that the three solar plants of combination A1 complement each other well on an annual scale, forming a steady power supply. Combinations A2 and A3, which have higher CV_{24} values, present a clear seasonal tendency since the wind farms produce more energy from June to September than in the rest of the year. Regarding the LCOH, this measure seems to play a minor role since combination A2 has the highest CV_{24}, but the lowest LCOH.

From these observations, the dispersion measured by the CV_h seems to be an important factor for the LCOH. However, comparing the indicators of combinations A1 and A3 from Table 5, it can be seen that A3 produces the most expensive hydrogen even though it has a lower CV_h than that of combination A1. Since LCOE of combination A3 is considerably higher than that of the other combinations, it can be inferred that LCOE is the second significant indicator.
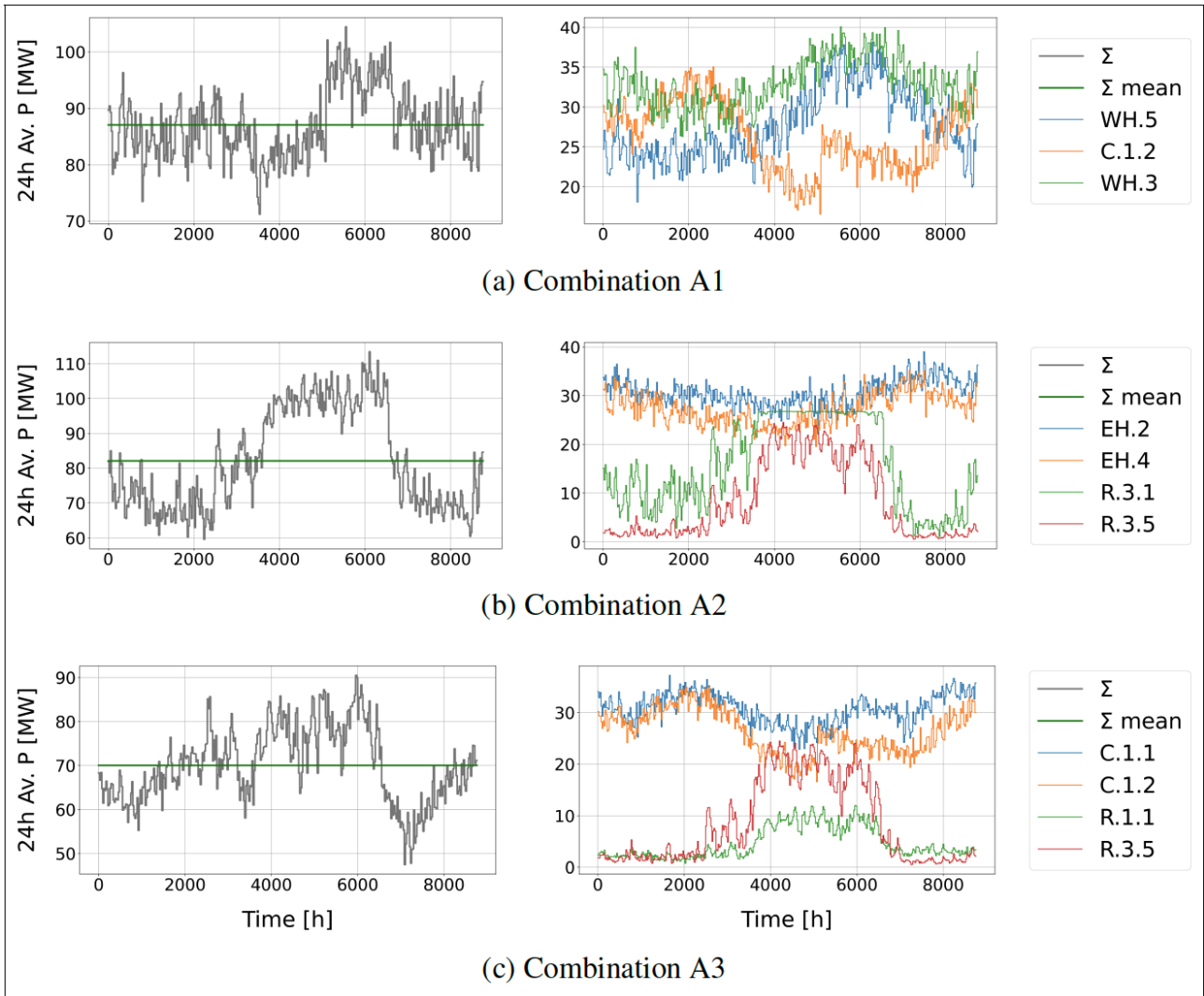
Fig. 4: *24-hour average power generation of the combinations A for one year. On the left, the total power output of the combined operation (gray line) and the annual mean (green line). On the right the power output per site.*

In Fig. 5, the power output is displayed together with the installed energy capacity (red line), and the operation schedule of the electrolyzers (green line). The green line hence shows the optimal operation identified by the optimizer, that yields the results presented in Table 5. It can be seen that the lowest production costs are generated if the installed electrolyzers operate whenever possible. These results differ from those of Varela et al. (2023), where the optimal generation involved reducing the electrolyzer power if the grid electricity is too expensive. In our case study, grid electricity is not considered and the only variable costs emerging are the startup and shutdown costs. Even though the grid energy fluctuates and causes many startup and shutdown cycles, the optimization has shown that each is economical.
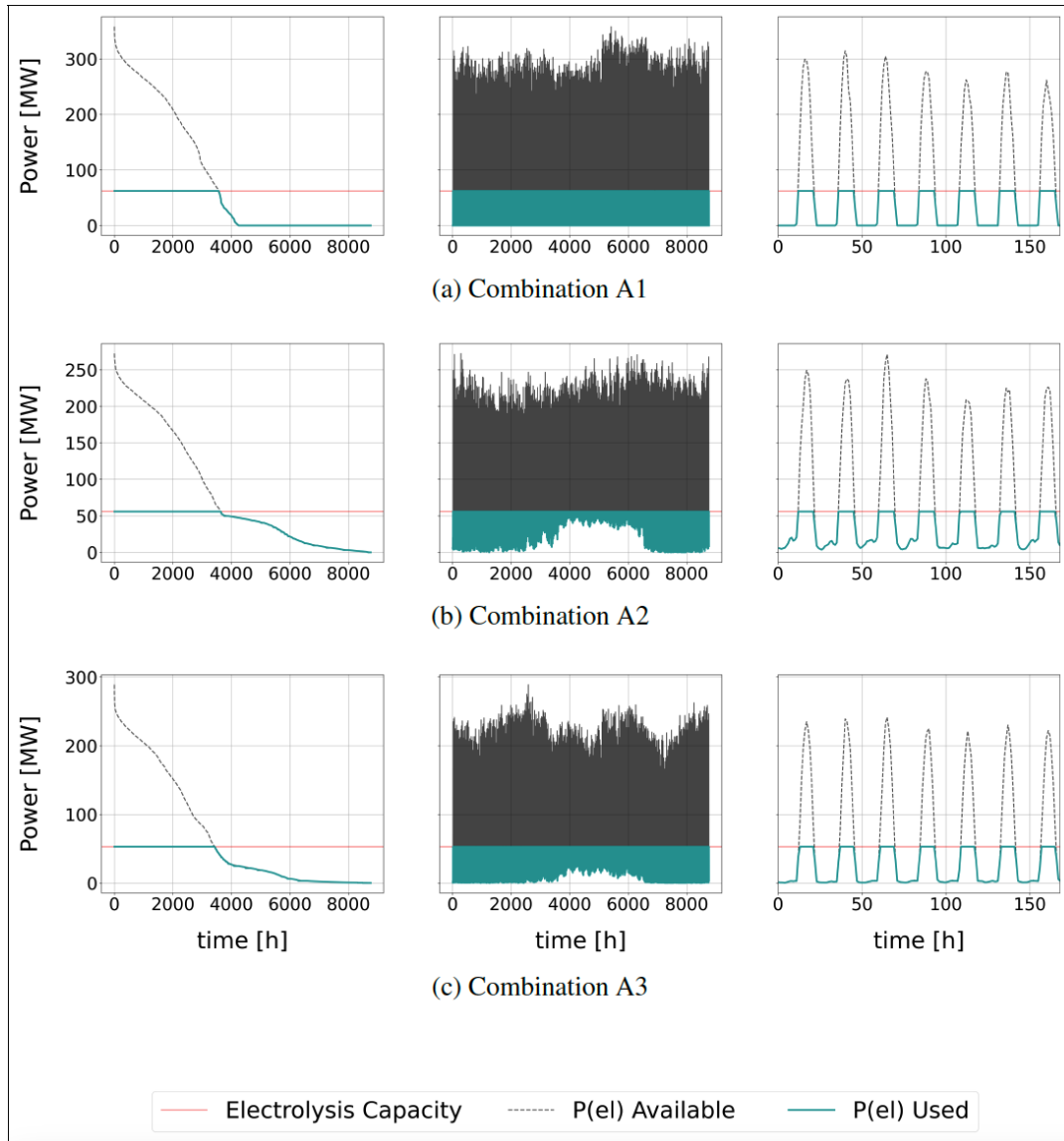
Fig. 5: *Power plant energy generation (gray line), electrolyzer energy use (green line), and installed electrolysis capacity (red line) of the combinations A. On the left as yearly duration curves, in the middle as feed-in time series for the whole year, and on the right as feed-in time series of the first week of the year.*

Conclusions and outlook

In this study, we evaluate the techno-economic conditions of green hydrogen production based on geographically-dispersed and complementary solar PV and wind power in Ecuador. We use hourly meteorological data of representative sites with high resource potential to simulated the power output. An electrolysis optimization model is used to simulate the hydrogen production based on the PV and wind power feed-in time series.

We use a set of indicators to evaluate the relation between the feed-in time series of the PV and wind power farms and the hydrogen production and cost. The selected indicators are coefficient of variation at hourly and daily timescales (CV_h and CV_{24}, respectively), levelized cost of electricity (LCOE), and full load hours (FLH). We test this approach on a sample of three site combinations to identify which factors are relevant to the cost of hydrogen production.

Based on the assumptions explained in this work, the three combinations of PV and wind power sites produce green hydrogen at a levelized cost of hydrogen (LCOH) of less than US$4 per kg. Regarding the indicators, the coefficient CV_h is found to be a helpful indicator. Results show that the lower the CV_h, the higher the stability of the renewable power output, and consequently the lower the LCOH. Another indicator that proved to be relevant is the LCOE, since results indicate that the lower the cost for the electric energy, the lower the cost for the hydrogen. It is also observed that generation sites that support power plant operations for more FLHs have lower LCOE. This stresses the importance of

the usage of sites with a high renewable resource potential. The seasonal stability measured by the coefficient CV_{24} does not seem to influence the LCOH significantly. This is because it omits the high daily fluctuations of the solar farms, which influence the electrolysis generation substantially.

Since we only evaluate three of more than a million possible combinations, future work will be focused on evaluating more combinations of solar and wind power farms. This will be useful to determine whether the production based on other combinations can generate better results in terms of LCOH. For this, we will use the two indicators: CV_h and LCOE, which seem to influence the LCOH in this study, to identify more promising site combinations. Future work will also include a sensitivity analysis to assess how the variation of input parameters for the simulation of the renewable power and the electrolysis have an impact on the calculated LCOH.

Authors contribution

Sven Kock: Conceptualization, methodology, software, visualization, formal analysis, investigation, validation, writing–original draft, writing–review and editing. **Mariela Tapia:** Conceptualization, methodology, software, supervision, writing–original draft, writing–review and editing
Christopher Varela: Conceptualization, software, supervision, writing–review and editing. **Matthias Schirmer:** Supervision, writing–review and editing.

References

Abdin, Z., Zafaranloo, A., Rafiee, A., Mérida, W., Lipiński, W., & Khalilpour, K. R. (2020). Hydrogen as an energy vector. *Renewable and Sustainable Energy Reviews*, *120*, 109620.

Alavijeh, M. K., Yaghmaei, S., & Mardanpour, M. M. (2020). Assessment of Global Potential of Biohydrogen Production from Agricultural Residues and Its Application in Nitrogen Fertilizer Production. *BioEnergy Research*, *13*(2), 463–476. https://doi.org/10.1007/s12155-019-10046-1

Anderson, K. S., Hansen, C. W., Holmgren, W. F., Jensen, A. R., Mikofski, M. A., & Driesse, A. (2023). pvlib python: 2023 project update. *Journal of Open Source Software*, *8*(92), 5994. https://doi.org/10.21105/joss.05994

ARCERNNR. (2024). *Estadística anual y multianual del sector eléctrico ecuatoriano 2023*. http://www.controlrecursosyenergia.gob.ec/estadistica-del-sector-electrico/

Behrends, E. (2013). Kombiniere! In *Fünf Minuten Mathematik: 100 Beiträge der Mathematik-Kolumne der Zeitung DIE WELT* (pp. 80–83). Springer Fachmedien Wiesbaden. https://doi.org/10.1007/978-3-658-00998-4_29

Bockelmann, M., Becker, M., Stypka, S., Bauer, S., Minke, C., & Turek, T. (2024). Erzeugung von Wasserstoff durch Elektrolyse. *Chemie in unserer Zeit*, *58*(1), 29–45. https://doi.org/10.1002/ciuz.202300024

CONELEC. (2008). *Atlas solar del Ecuador con fines de generación eléctrica*. Consejo Nacional de Electricidad.

Decker, M., Schorn, F., Samsun, R. C., Peters, R., & Stolten, D. (2019). Off-grid power-to-fuel systems for a market launch scenario – A techno-economic assessment. *Applied Energy*, *250*, 1099–1109. https://doi.org/10.1016/j.apenergy.2019.05.085

Dobos, A. (2014). PVWatts Version 5 Manual—Technical Report NREL/TP-6A20-62641. In *National Renewable Energy Laboratory* (No. September; p. 20). https://www.nrel.gov/docs/fy14osti/62641.pdf

European Central Bank. (2024, August 2). *Euro foreign exchange reference rates—US dollar*. https://www.ecb.europa.eu/stats/policy_and_exchange_rates/euro_reference_exchange_rates/html/usd.xml

González, P. (2024, April 24). *Cortes de luz ya dejan USD 576 millones en pérdidas para Ecuador*. Primicias. https://www.primicias.ec/noticias/economia/perdidas-cortes-luz-economia-empresas/

Haas, S., Krien, U., Schachler, B., Bot, S., Zeli, V., Maurer, F., Shivam, K., Witte, F., Rasti, S. J., Seth, & Bosch, S. (2024). *wind-python/windpowerlib: Update release* (Version v0.2.2) [Computer software]. Zenodo. https://doi.org/10.5281/zenodo.10685057

Hartung, J., Elpelt, B., & Klösener, K.-H. (2005). *Statistik: Lehr- und Handbuch der angewandten Statistik ; mit zahlreichen, vollständig durchgerechneten Beispielen* (14., unwesentlich veränd. Aufl). Oldenbourg.

Hay, J. E., & Davies, J. A. (1980). Calculation of the solar radiation incident on an inclined surface. *Proceedings of the 1st Canadian Solar Radiation Data Workshop*, 59–72.

IHA. (2017). *Hydropower Status Report 2017*. International Hydropower Association. https://www.hydropower.org/resources/publications

IHA. (2021, May 25). *New paper: Couple green hydrogen with hydropower to create a net zero future*. https://www.hydropower.org/news/the-green-hydrogen-revolution-hydropowers-transformative-role

IRENA. (2023). *Renewable power generation costs in 2022*. International Renewable Energy Agency. https://www.irena.org/-/media/Files/IRENA/Agency/Publication/2023/Aug/IRENA_Renewable_power_generation_costs_in_2022.pdf

JaSolar. (n.d.). *605W MBB Half-cell Module JAM78S30 580-605/MR*. https://www.jasolar.com/uploadfile/2022/0224/20220224053234854.pdf

Kost, C., Shammugam, S., Fluri, V., Peper, D., Davoodi Memar, A., & Schlegl, T. (2021). *Stromgestehungskosten Erneuerbare Energien*. Fraunhofer-Institute for Solar Energy Systems ISE. https://www.ise.fraunhofer.de/content/dam/ise/de/documents/publications/studies/DE2021_ISE_Studie_Stromgestehungskosten_Erneuerbare_Energien.pdf

MEER. (2013). *Atlas Eólico del Ecuador con fines de generación eléctrica*. Ministerio de Electricidad y Energía Renovable.

Mermoud, A. (2014). *PVsyst (Version 6.23)* [Computer software]. ISE, University of Geneva. http://www.pvsyst.com

MERNNR. (2018). *Plan Maestro de Electricidad 2018-2027*. Ministerio de Energía y Recursos Naturales no Renovables.

Mertens, K. (2020). *Photovoltaik: Lehrbuch zu Grundlagen, Technologie und Praxis* (5., aktualisierte Auflage). Hanser.

Ministerio de Energía y Minas. (2023, July). *Hoja de Ruta del Hidrógeno Verde en Ecuador*. https://www.recursosyenergia.gob.ec/wp-content/uploads/2023/11/hoja_de_ruta_hidrogeno_verde_Modificado.pdf

Müller-Markus, C., Mitrovic, M., Schlögl, R., Schmidt, C., Merz, M., Lemmer, K., Lüke, W., Iwan, N., Green, P., Fendl, S., Winter-Berke, D., Abdelmessih, N., & Grenzebach, E. (2023). *Hydrogen*. Acatech - German Academy of Science and Engineering. https://doi.org/10.48669/horizonte_2023-2

Oliveira, A. M., Beswick, R. R., & Yan, Y. (2021). A green hydrogen economy for a renewable energy society. *Current Opinion in Chemical Engineering*, *33*, 100701. https://doi.org/10.1016/j.coche.2021.100701

Sauer, K. J., Roessler, T., & Hansen, C. W. (2015). Modeling the Irradiance and Temperature Dependence of Photovoltaic Modules in PVsyst. *IEEE Journal of Photovoltaics*, *5*(1), 152–158. https://doi.org/10.1109/JPHOTOV.2014.2364133

Sengupta, M., Xie, Y., Lopez, A., Habte, A., Maclaurin, G., & Shelby, J. (2018). The National Solar Radiation Data Base (NSRDB). *Renewable and Sustainable Energy Reviews*, *89*, 51–60. https://doi.org/10.1016/J.RSER.2018.03.003

SMA. (n.d.). *Sunny Central UP*. https://www.jasolar.com/uploadfile/2022/0224/20220224053234854.pdf

Smith, C., Hill, A. K., & Torrente-Murciano, L. (2020). Current and future role of Haber–Bosch ammonia in a carbon-free energy landscape. *Energy & Environmental Science*, *13*(2), 331–344.

Staffell, I., & Green, R. (2014). How does wind farm performance decline with age? *Renewable Energy*, *66*, 775–786. https://doi.org/10.1016/j.renene.2013.10.041

Steffen, B. (2020). Estimating the cost of capital for renewable energy projects. *Energy Economics*, *88*, 104783. https://doi.org/10.1016/j.eneco.2020.104783

Tapia, M. (2023). *Variability analysis of renewable power generation in complex terrain and the contribution of the spatio-temporal synergies for a resilient power supply. Methodology development and Ecuador case study* [PhD Thesis, Universität Bremen]. https://doi.org/10.26092/elib/2780

Tapia, M., Heinemann, D., Ballari, D., & Zondervan, E. (2022). Spatio-temporal characterization of long-term solar resource using spatial functional data analysis: Understanding the variability and complementarity of global horizontal irradiance in Ecuador. *Renewable Energy*, *189*, 1176–1193. https://doi.org/10.1016/j.renene.2022.03.049

Tapia, M., Ramos, L., Heinemann, D., & Zondervan, E. (2022). Power to the city: Assessing the rooftop solar photovoltaic potential in multiple cities of Ecuador. *Physical Sciences Reviews*, *8*(9), 2285–2319. https://doi.org/10.1515/psr-2020-0061

Umweltbundesamt. (2023, December 21). *Photovoltaik-Freiflächenanlagen*. https://www.umweltbundesamt.de/themen/klima-energie/erneuerbare-energien/photovoltaik/photovoltaik-freiflaechenanlagen#flacheninanspruchnahme-durch-photovoltaik-freiflachenanlagen

Van Sark, W. G. J. H. M., Van der Velde, H. C., Coelingh, J. P., & Bierbooms, W. A. A. M. (2019). Do we really need rotor equivalent wind speed? *Wind Energy*, *22*(6), 745–763. https://doi.org/10.1002/we.2319

Varela, C., Mostafa, M., & Zondervan, E. (2023). Optimal production of green hydrogen with grid assistance for enhanced flexibility. *Computer Aided Chemical Engineering*, *52*, 2917–2922. https://doi.org/10.1016/B978-0-443-15274-0.50464-9

Wang, Y., Chao, Q., Zhao, L., & Chang, R. (2022). Assessment of wind and photovoltaic power potential in China. *Carbon Neutrality*, *1*(1), 15. https://doi.org/10.1007/s43979-022-00020-w

Wesselak, V., & Schabbach, T. (2009). *Handbuch Regenerative Energietechnik*. Springer.